

# TS-CGNet: Temporal-Spatial Fusion Meets Centerline-Guided Diffusion for BEV Mapping

Xinying Hong<sup>1</sup>, Siyu Li<sup>2</sup>, Kang Zeng<sup>1</sup>, Hao Shi<sup>3</sup>, Bomin Peng<sup>2</sup>, Kailun Yang<sup>2,\*</sup>, and Zhiyong Li<sup>1,2,\*</sup>

**Abstract**—Bird’s Eye View (BEV) perception technology is crucial for autonomous driving, as it generates top-down 2D maps for environment perception, navigation, and decision-making. Nevertheless, the majority of current BEV map generation studies focusing on visual map generation lack depth-aware reasoning capabilities. They exhibit limited efficacy in managing occlusions and handling complex environments, with a notable decline in perceptual performance under adverse weather conditions or low-light scenarios. Therefore, this paper proposes TS-CGNet, which leverages Temporal-Spatial fusion with Centerline-Guided diffusion. This visual framework, grounded in prior knowledge, is designed for integration into any existing network for building BEV maps. Specifically, this framework is decoupled into three parts: Local mapping system involves the initial generation of semantic maps using purely visual information; The Temporal-Spatial Aligner Module (TSAM) integrates historical information into mapping generation by applying transformation matrices; The Centerline-Guided Diffusion Model (CGDM) is a prediction module based on the diffusion model. CGDM incorporates centerline information through spatial-attention mechanisms to enhance semantic segmentation reconstruction. We construct BEV semantic segmentation maps by our methods on the public nuScenes and the robustness benchmarks under various corruptions. Our method improves 1.90%, 1.73%, and 2.87% for perceived ranges of  $60 \times 30m$ ,  $120 \times 60m$ , and  $240 \times 60m$  in the task of BEV HD mapping. TS-CGNet attains an improvement of 1.92% for perceived ranges of  $100 \times 100m$  in the task of BEV semantic mapping. Moreover, TS-CGNet achieves an average improvement of 2.92% in detection accuracy under varying weather conditions and sensor interferences in the perception range of  $240 \times 60m$ . The source code will be publicly available at <https://github.com/krabs-H/TS-CGNet>.

## I. INTRODUCTION

Bird’s Eye View (BEV) perception technology has emerged as a critical component in autonomous driving systems, primarily focusing on constructing comprehensive 2D top-down representations [1], [2]. This technology plays a fundamental role in enabling essential autonomous functions including real-time environment perception, path planning, and strategic decision-making. Semantic mapping is crucial for constructing BEV maps, as it encodes critical environ-

This work was supported in part by the National Natural Science Foundation of China (No. U21A20518, No. 61976086, and No. 62473139) and in part by Hangzhou SurImage Technology Company Ltd.

<sup>1</sup>X. Hong, K. Zeng, and Z. Li are with the College of Computer Science and Electronic Engineering, Hunan University, Changsha 410082, China.

<sup>2</sup>S. Li, B. Peng, K. Yang, and Z. Li are with the School of Robotics and the National Engineering Research Center of Robot Visual Perception and Control Technology, Hunan University, Changsha 410082, China.

<sup>3</sup>S. Hao is with the State Key Laboratory of Extreme Photonics and Instrumentation, Zhejiang University, Hangzhou 310027, China.

\*Corresponding authors (e-mail: kailun.yang@hnu.edu.cn, zhiyong.li@hnu.edu.cn).

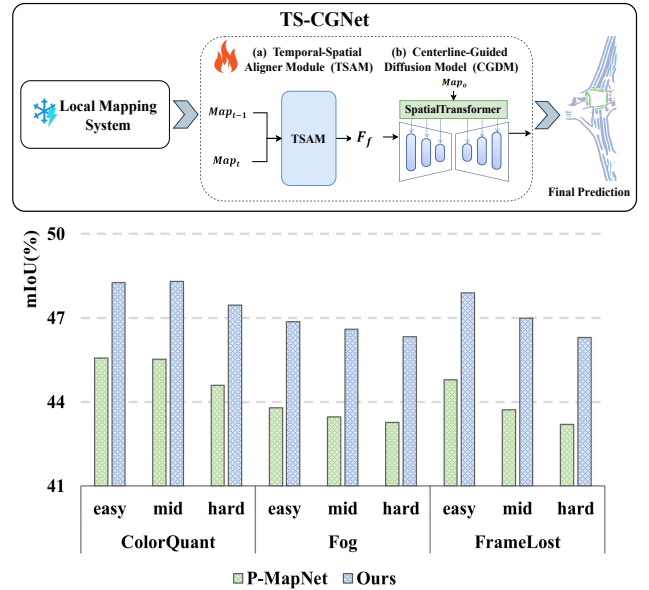


Fig. 1: Overview of TS-CGNet, the proposed framework for BEV semantic mapping using historical and centerline priors. In addition, the bar chart illustrates the robustness under varying environments and sensor influences between ours and the state-of-the-art method [5].

mental semantics and provides rich semantic details. Its precision directly impacts navigation reliability and decision-making robustness, significantly enhancing the utility of BEV semantic maps in autonomous driving and intelligent transportation systems [3], [4].

Owing to the absence of depth-aware reasoning, existing BEV map generation schemes [6] often result in information loss when converting perspective views to BEV space, generating maps with problems such as gaps and discontinuities. The primary cause of this phenomenon is the sparsity of visual information. Particularly in complex scenarios (*i.e.* adverse weather conditions), the robustness of visual information is significantly compromised, leading to diminished accuracy in BEV maps. In addition, existing methods [7] tend to rely only on the image acquired in the current frame for map construction, neglecting the important role of prior information in map generation.

The prior information has been widely applied in the field of map construction, such as P-MapNet [5]. It significantly improves model performance by fusing the prior information from Standard-Definition Maps (SDMap) and High-Definition Maps (HDMap). Despite high precision in map generation technology, its robustness is notably lacking, particularly under severe weather conditions where its

performance necessitates further enhancement. We observe that temporal information can also be used as a kind of prior information, which can make up for the gap in the map caused by the sparsity of the current frame. Therefore, this paper proposes a purely vision-based framework to assist map reconstruction and leverages historical frame maps and centerlines as the prior information for enhancing the completeness and continuity of the generated maps.

As shown in Fig. 1, this paper introduces TS-CGNet which contains three parts, aiming to explore how to improve the effectiveness of BEV maps from a purely visual perspective with information captured by cameras. **Local Mapping System** is responsible for the initial generation of semantic maps using purely visual data. **Temporal-Spatial Aligner Module (TSAM)** leverages historical frame data to enrich the current frame. Historical frames often contain critical information that may be absent in the current frame. By integrating this supplementary data, the completeness of environmental information is significantly enhanced. **Centerline-Guided Diffusion Model (CGDM)** is a diffusion-based generative model conditioned on centerlines. The centerlines, as important prior knowledge in map generation, are embedded to capture key features more accurately through partial attention in the denoising network.

Extensive experiments on the public nuScenes dataset [8] and the robustness benchmarks [9] demonstrate that our method has a great capacity to reconstruct BEV semantic maps. TS-CGNet achieves gains of 1.9%, 1.73%, and 2.87% for perceived ranges of  $60\times 30m$ ,  $120\times 60m$ , and  $240\times 60m$ , respectively. When subjected to various weather and sensor factors, it further improves by an average of 2.92% for the  $240\times 60m$  range.

The contributions of this work are summarized as follows.

- 1) Put forward TS-CGNet, which serves as a new solution for BEV semantic mapping construction by proposing modules that can handle various map construction tasks.
- 2) Propose *Temporal-Spatial Aligner Module (TSAM)*, which aligns historical prior information to the current using vehicle translation information and angle transformation. This process supplements the current frame maps, thereby enhancing the completeness and reliability of the current map generation elements.
- 3) Design *Centerline-Guided Diffusion Model (CGDM)*, which utilizes centerlines to guide the recovery and generation of high-precision maps from noise. It focuses on road details during the map generation process, thereby significantly improving the accuracy of the resulting maps.

## II. RELATED WORK

### A. Camera-Based BEV Mapping System

Significant progress was made in semantic segmentation maps under the pure vision domain. A multi-camera setup was used to reconstruct 3D scenes and project them onto a BEV plane. The BEV region was rasterized and subsequently

classified at the cellular level using a convolutional neural network [10]. Methods like LSS [11] and IPM [12] converted image features to BEV space by depth estimation. BEVFusion [1] fused features from cameras and LiDAR in the BEV space for tasks like 3D object detection and map segmentation. BEVFormer [2] aggregated multi-view camera features and historical BEV features using spatio-temporal attention. HDMapNet [7] transformed perspective view features into BEV space using neural view transformation and generated semantic segmentation maps through a segmentation head. Some works [13]–[16] focused on effectively learning BEV features to enhance perception and improve map quality.

### B. Use Prior Knowledge to Generate Maps

Leveraging prior knowledge for BEV map construction [4] [17] boosted autonomous driving perception, robustness, and map generation accuracy, facilitating generalization across scenarios and continuous global map updates. Commonly used prior knowledge included historical map priors and standard definition maps.

Standard Definition Maps (SDMap) offer a lightweight road topology at a low maintenance cost. OpenStreetMap (OSM) [18], a widely used public dataset, aids online map prediction and lane understanding, improving lane detection and topology prediction. However, it occasionally encounters alignment discrepancies with high-definition maps. To achieve significant performance improvements, P-MapNet [5] incorporated weakly aligned SDMap prior into the online map generator by attention-based architecture. BLOS-BEV [19] fused visual and map features to achieve BEV segmentation beyond the scope of previous methods.

Despite the success of single-frame methods in high-definition map construction, they still struggled with complex scenes and occlusions, highlighting the need for local prior knowledge. Therefore, historical prior knowledge has become a research priority. NMP [20], as the first learning-based system to create a global map prior, constructed a global map prior from previous traversals to enhance the map prediction. StreamMapNet [21] used a streaming strategy for temporal fusion, preserving temporal info by propagating hidden states through frames. GlobalmapNet [22], the initial online framework for constructing vectorized global high-precision maps, facilitated continuous map updates and ensured prediction consistency. DTCLMapper [23] revisited the temporal fusion of vector HD maps on post-processing, focusing on temporal instance consistency and temporal map consistency learning. Intriguingly, although both map priors and temporal priors have been demonstrated to enrich mapping performance, there is a paucity of research exploring their combined potential.

Consequently, we propose an engaging inquiry, questioning whether the interplay between these two can yield complementary effects that enhance mapping efficacy.

### C. Generate Maps with Diffusion Models

Generative learning models were essential for BEV map construction. It learned efficiently from limited sensor data

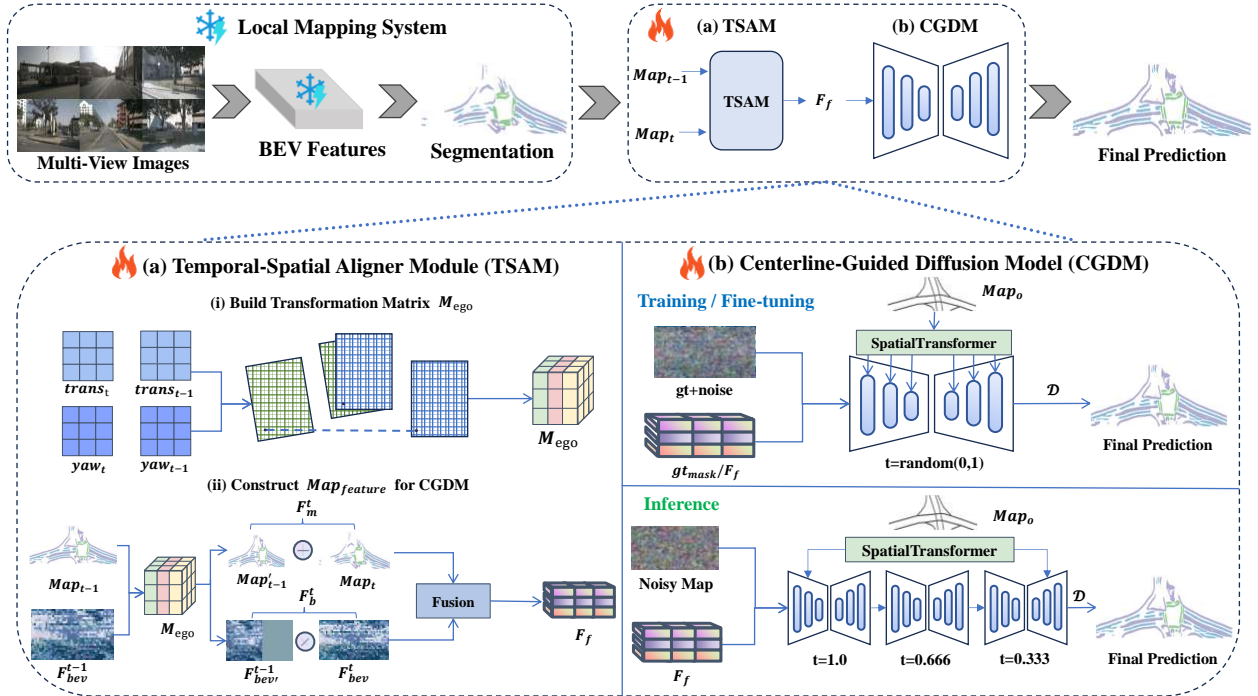


Fig. 2: The structure of TS-CGNet. It consists of a local mapping system, the temporal-spatial aligner module, and the centerline-guided diffusion model. Integrating historical maps can provide additional prior knowledge, allowing the diffusion model to fit a more comprehensive map distribution.

to generate detailed, high-resolution, multi-view maps. In this area, Variational Autoencoder (VAE) [24], [25] used variational inference to model the latent space, whereas Autoregressive models [26] broke down complex generative problems into a series of simpler conditional generation tasks. Masked Auto-Encoders (MAE) [16], [27] were scalable self-supervised models for image and video generation, masking, and reconstructing the input images. MapPrior [28] integrated a traditional discriminative BEV perceptual model with a learned generative semantic map layout model, addressing the limitations of existing models in producing realistic and consistent semantic map layouts. Recently, diffusion models [29], [30], including Stable Diffusion [31], generated high-quality images from the text by denoising in a low-dimensional latent space, improving efficiency and lowering computational expenses. ControlNet [32] directed pre-trained diffusion models with varied conditional inputs to produce tailored images. The DDP framework [6], leveraging conditional diffusion models, excelled in tasks like semantic segmentation and depth estimation. It was progressively denoised to generate predictions, utilizing a discrete latent space for robust, efficient sampling. DiffMap [33] was designed to model the structured priors of map segmentation masks using latent diffusion models. However, the advantages of prior knowledge were not fully considered in map generation.

In contrast to these existing methods, TS-CGNet appears as the first network to consider both OSM and historical priors as prior knowledge. It is a framework capable of handling various BEV map construction tasks.

### III. METHODOLOGY

Currently, BEV map generation techniques are prone to feature loss when mapping BEV features to maps. This ultimately leads to gaps, discontinuities, and other problems in the generated maps, seriously affecting their accuracy and completeness. However, most existing research on purely visual map generation schemes tends to be deficient in depth-aware reasoning, poorly adaptable to occlusion and complex scenes, and substantially downgraded in perceptual capabilities under bad weather or low-light conditions. Therefore, we propose a scheme based on pure vision, where diverse prior information serves as a solution to address the aforementioned challenges. The scheme consists of three parts as shown in Fig. 2:

- 1) A **Local Mapping System** (Sec. III-A) generates current frame maps via fixed-parameter encoders and decoders, which is a flexibly embeddable module.
- 2) The proposed **Temporal-Spatial Aligner Module (TSAM)** (Sec. III-B) enriches the learnable information of the current frame by integrating temporal knowledge at both the map and feature levels.
- 3) The designed **Centerline-Guided Diffusion Model (CGDM)** (Sec. III-C) uses road centerline knowledge to guide map generation via spatial attention, improving map accuracy and efficiency.

#### A. Local Mapping System.

Various BEV mapping tasks [7] [11] [13] can fit into the local mapping system. Generally, BEV mapping is divided into three steps: image encoding, BEV feature encoder, and map decoder.

**Image encoder.** Image encoding takes multi-view images as input to learn two-dimensional semantic features and spatial relationships. Each image  $I_i$  is embedded in a shared neural network  $\phi_I$  to obtain the perspective feature  $F_{I_i}^{pv} \subseteq \mathbb{R}^{H_{pv} \times W_{pv} \times K}$ ,  $H_{pv}$ ,  $W_{pv}$ , and  $K$  indicate height, width and channel, respectively.

**BEV feature encoder.** Given the geometric discrepancy between perspective views and BEV, conventional methods typically employ explicit/implicit depth estimation learned from two-dimensional spatial relationships to facilitate the transformation between different views. In the field of BEV mapping, Inverse Perspective Mapping (IPM) [12] is a widely-recognized view-transformation technique, attributed to its generalization capability. Thus, IPM is used for the feature extraction module in this local mapping system.

**Map decoder.** Finally, the decoder module is utilized to obtain BEV mapping results, such as semantic high-definition maps. The map decoder is a Fully Convolutional Network (FCN) [34] that receives the BEV features extracted from images captured by 6 surrounding cameras as input. By employing a segmentation head, the map decoder is capable of categorizing road information.

### B. Temporal-Spatial Aligner Module

Due to the susceptibility of current single-frame maps to environmental changes, such as sensor impairments, issues of incomplete BEV maps often arise. The history frame information records the past environment states, which may contain details and features missing in the current frame. Therefore, we contemplate whether prior knowledge can be utilized to refine the map. Therefore, this paper proposes the Temporal-Spatial Aligner Module (TSAM), which can accurately map the information in the historical prior to the corresponding position of the current frame, to supplement the features of the current frame, which can be categorized into map-level fusion and feature-level fusion.

**Map-level fusion.** This part addresses the BEV maps of consecutive frames,  $\text{Map}_t$  and  $\text{Map}_{t-1}$ . Initially, the self-motion transformation matrix  $M_{ego} \in \mathbb{R}^{3 \times 3}$  of the vehicle is employed to align the two frames of the map.

$$\text{Map}_{t-1} = \text{Plane}((X_i, Y_i), \dots, (X_h, Y_w)), \quad (1)$$

$$\begin{bmatrix} X'_i \\ Y'_i \\ 1 \end{bmatrix} = M_{ego} \cdot \begin{bmatrix} X_i \\ Y_i \\ 1 \end{bmatrix}, \quad (2)$$

$$\text{Map}'_{t-1} = \text{Plane}((X'_i, Y'_i), \dots, (X'_h, Y'_w)), \quad (3)$$

where the BEV plane is divided into independent small grids, representing  $(X_i, Y_i)$  in the ego coordinate system.  $\text{Plane}$  represents the set of all BEV grids.

Then, the aligned historical map  $\text{Map}'_{t-1}$  and the current map are summed and convolved to realize fusion. The scheme for fusion is as follows:

$$F_m = \text{RELU} \left( \varphi_1(\text{Map}'_{t-1} + \text{Map}_t) \right), \quad (4)$$

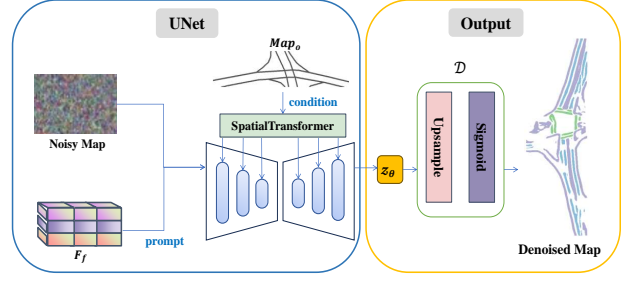


Fig. 3: The framework of CGDM. It integrates  $F_f$  as the prompt and  $\text{Map}_o$  as the condition into the UNet decoder to refine noisy features into accurate BEV maps.

$F_m$  indicates the map features that were aligned for feature fusion and  $\varphi_i$  means the  $i$ -th layer of  $3 \times 3$  convolution. ReLU denotes the rectified linear unit activation.

**Feature-level fusion.** Despite the integration of historical maps, the informational content conveyed by the map remains somewhat limited, transmitting only unidirectional semantic information. Therefore, we further explore the utilization of BEV features to provide richer prior knowledge. Here, we also integrate historical feature information. Unlike the map fusion, the concatenate operation followed by convolution is used to realize fusion depicted as follows:

$$F_b = \varphi_2(\text{Concat}(\text{Aligned}(M_{ego}, F_{bev}^{t-1}), F_{bev}^t)), \quad (5)$$

where  $F_b$  indicates the fused feature,  $F_{bev}^{t-1}$  and  $F_{bev}^t$  represent the feature from the previous and current local mapping system.  $\text{Aligned}(\cdot)$  is an alignment operation, as shown in Eq. 1 to Eq. 3.

Finally, the features obtained from both layers are fused into a complete feature  $F_f$ , obtaining rich characterization of semantic mapping that helps the diffusion model recover pure noise:

$$F_f = \varphi_3(F_m + F_b). \quad (6)$$

### C. Centerline-Guided Diffusion Model

To generate more comprehensive BEV maps with the help of temporal multi-layer features, the diffusion model, recognized as a high-quality generative model, is selected for CGDM. If BEV maps are generated solely from fused temporal features, the diffusion model will rely exclusively on dataset fitting, potentially leading to issues such as weak robustness. Therefore, we have designed a mapping diffusion model guided by centerline information, where the centerline data is sourced from OSM, as shown in Fig. 3.

During the learning process, the ground truth  $y_i$ , temporally fused features  $F_f$ , and OSM  $\text{Map}_o$ , serve as input objects. First, the ground truth  $y_i$  is encoded into the latent space by the encoder  $\varepsilon$  to perform the enhancements:

$$z = \varepsilon(y_i), \quad (7)$$

where  $z \in \mathbb{R}^{D \times H \times W}$ . Next the Gaussian noise  $\sigma$  is added through a diffusion process  $\{z_t\}_{t=0}^T$  at each time step  $t$ , where  $z_0 = z$ .

TABLE I: Quantitative results of BEV HD maps on nuScenes [8]. ‘S’ means OSM, whereas ‘H’ stands for using HD maps. \* represents data from the reference paper.

Range (m)	Method	S	S+H	Epoch	Div.	Ped.	Bound.	mIoU (%)
60×30	HMapNet* [7]			30	40.50	19.70	40.50	33.57
	DiffMap* [33]			30	42.10	23.90	42.20	36.07
	P-MapNet [5]	✓	✓	10	44.30	23.30	43.80	37.13
	Baseline	✓		30	44.10	22.60	43.80	36.83
	Ours	✓	✓	10	45.90	25.80	45.40	39.03
	<b>Improvement (%)</b>	-	-	-	<b>+1.60</b>	<b>+2.40</b>	<b>+1.60</b>	<b>+1.90</b>
120×60	HMapNet* [7]			30	39.20	23.00	39.10	33.77
	P-MapNet [5]	✓	✓	10	45.50	30.90	46.20	40.87
	Baseline	✓		30	44.80	30.60	45.60	40.33
	Ours	✓	✓	10	47.30	33.20	47.30	42.60
	<b>Improvement (%)</b>	-	-	-	<b>+1.80</b>	<b>+2.30</b>	<b>+1.10</b>	<b>+1.73</b>
240×60	HMapNet* [7]			30	31.90	17.00	31.40	26.77
	P-MapNet [5]	✓	✓	10	49.00	40.90	46.60	45.50
	Baseline	✓		30	46.30	35.70	44.60	42.20
	Ours	✓	✓	10	51.60	43.90	49.60	48.37
	<b>Improvement (%)</b>	-	-	-	<b>+2.60</b>	<b>+3.00</b>	<b>+3.00</b>	<b>+2.87</b>

Then the latent feature with added noise  $z_n$  and the fused temporal feature  $F_f$  are intermingled, serving as generative features to be mined. Under the guidance of the OSM  $Map_o$ , the map features  $z_\theta$  can be generated from the noise features.

$$z_\theta = M(z_n, F_f, Map_o), \quad (8)$$

where  $M$  is the core network for predicting noise during the denoising process model based on the UNet [35] structure.  $M$  consists of 27 modules, with 8 of them dedicated to up-sampling and downsampling operations to adjust the feature map sizes. Among the remaining processing modules, the 15 modules are composed of ResBlocks [31] and Spatial Transformers [36], which are concatenated via skip connections. The ResBlocks [31] mitigate vanishing gradients via residual learning, safeguarding input feature integrity. The Spatial Transformers [36] facilitate spatial invariance with dynamic transformations. The central 4 modules retain the original ResBlock [31] design to ensure stability and consistency in the core region, further improving feature propagation. This setup allows the model to concentrate on centerline details by leveraging OSM data to guide the generation process. It achieves a conditional fusion of multi-scale features by dynamically generating spatial attention masks and conditional vectors, which focus on critical road semantic areas. Additionally, the model learns to identify and recover noise-related features, enhancing image accuracy.

Finally, after obtaining the initial prediction, we use up-sampling and sigmoid for the original pixel space as a BEV semantic map.

#### D. Loss Function.

For the supervision of the proposed model, the focal loss [37] is applied between the ground truth map  $y_i$  and

the predicted map  $\hat{y}_i$ :

$$Loss = \frac{1}{N} \sum_{i=1}^N (\text{BCE}(y_i, \hat{y}_i) \cdot (1 - p_{t_i})^\gamma), \quad (9)$$

where BCE is the computation of binary cross-entropy loss,  $p_{t_i}$  is the weighted sum of predicted probability and truth for each sample, and  $N$  is the number of semantic classes.

## IV. EXPERIMENTS

### A. Experimental Setup

**Datasets.** Extensive experiments on the public nuScenes dataset [8], OpenStreetMap (OSM) [18], and the robustness benchmarks [9] are conducted to investigate whether our method has a great ability to reconstruct BEV semantic maps. The nuScenes dataset [8] is a prominent benchmark in automated driving. It contains multi-view images and point clouds from 1000 scenes, divided into 700 for training, 150 for validation, and 150 for testing. It is further annotated with high-definition maps that include semantic labels, which are well-suited to our task requirements. In addition to training the model, during the pretraining of TS-CGNet, we employ 50% random masks of the ground truth as inputs. Additionally, we apply different visual perturbations to validate the robustness further. Here, the nuScenes-C dataset proposed in the work [9] is utilized as our dataset benchmark. It includes eight perturbations: *Brightness*, *CameraCrash*, *ColorQuant*, *Dark*, *Fog*, *FrameLost*, *MotionBlur*, *Snow*. The experimental results are subsequently evaluated to assess the generalization effects.

**Evaluation Metrics.** We evaluate the effectiveness of the proposed method on two tasks, BEV HD mapping, and BEV semantic mapping. *Divider (Div.)*, *Pedestrian Crossing (Ped.)*, and *Boundary (Bound.)* are included in BEV HD Mapping. *Drivable Area (Dri.)*, *Pedestrian Crossing (Ped.)*, *Walkway (Wal.)*, *Stop Line (Sto.)*, and *Car-Parking Area*

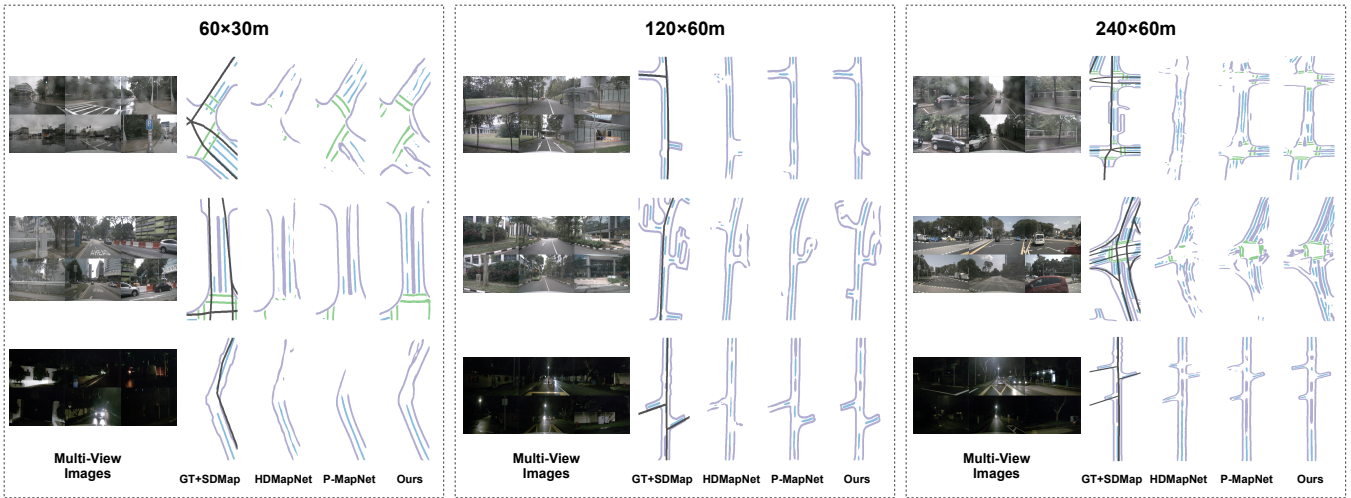


Fig. 4: The visualization of the BEV HD mapping task using TS-CGNet. The semantic colors indicate that ‘blue’ denotes (Div.), ‘green’ denotes (Ped.), and ‘purple’ denotes (Bound.).

TABLE II: Quantitative results of BEV map segmentation on nuScenes [8]. ‘VT’ means view transformer. ‘Gen’ indicates whether the generative mode is employed. \* represents data from the reference paper.

Methods	VT	Gen	OSM	Dri.	Ped.	Wal.	Sto.	Car.	Div.	mIoU (%)
OFT* [38]				74.00	35.30	45.90	27.50	35.90	33.90	42.08
LSS* [11]	LSS			75.40	38.80	46.30	30.30	39.10	36.50	44.40
DDP [6]	IPM	✓		75.90	39.00	46.10	32.40	38.70	30.20	43.72
P-MapNet [5]	IPM	✓	✓	76.00	39.00	47.80	33.90	39.80	34.00	45.08
Ours	IPM	✓	✓	<b>76.80</b>	<b>42.20</b>	<b>49.90</b>	<b>36.10</b>	<b>42.10</b>	<b>34.90</b>	<b>47.00</b>

(Car.), and Divider (Div.) are considered in BEV Semantic Mapping. The Intersection over Union (IoU) metric is applied as the validation criterion across all tasks. The IoU between the prediction and the ground truth is given by:

$$IoU(M_p, M_g) = \frac{|M_p \cap M_g|}{|M_p \cup M_g|}, \quad (10)$$

where  $M_p$  and  $M_g$  are the semantic prediction and the ground truth. These evaluation methods precisely compare our suitability for segmentation across different category sets. **Implementation Details.** For the BEV HD mapping task, we establish 3 perception ranges along the driving direction:  $60m \times 30m$  with  $0.15m$  for the short-range resolution,  $120m \times 60m$ , and  $240m \times 60m$  with  $0.3m$  for these two longer ranges. For the BEV semantic mapping task, the perception range is set at  $100m \times 100m$  with a map resolution of  $0.5m$ . The training is performed on a single RTX A6000 GPU with a batch size of 8 and a learning rate of  $1e-4$ . For learning rate scheduling, the Adam optimizer [12] is used with StepLR to schedule the learning rate tuning.

**Training.** The entire training process is divided into two phases. The first phase is pre-training, the diffusion model simulates the noise distribution on the ground truth data accompanied by 50% masks. This process is trained for 20 epochs, allowing the model to learn the missing features by masking at different positions in each iteration. In the subsequent 10 epochs of fine-tuning, the diffusion model learns from the map features aligned by TSAM to better reconstruct the BEV semantic maps.

TABLE III: Ablation results on different modules. We use  $120 \times 60m$  to assess the effectiveness.

Methods	Div.	Ped.	Bound.	mIoU (%)
Baseline	44.80	30.60	45.60	40.33
TS	46.20	33.30	46.80	42.10
CG	46.40	31.40	46.00	41.33
TS-CG	<b>47.30</b>	<b>33.20</b>	<b>47.30</b>	<b>42.60</b>

**Inference.** Given  $F_f$  as prompt and  $Map_o$  as conditions, the model begins with a random noise map sampled from a Gaussian distribution. With a step size of 3, the value of  $t$  is progressively decreased from 1.0 to 0.666, then to 0.333, and finally to 0, gradually denoising to generate a clear and complete map element image. We select the DDIM update rule for sampling. At each sampling step  $t$ , the random noise  $z_T$  from the last step or the predicted noise map  $z_{T-1}$  is fused with the prompt and conditional feature and passed to CGDM for map construction.

## B. Results and Visualization

**BEV HD Mapping.** We conduct a comparative analysis of different methods, e.g. HDMaNet [7], DiffMap [33], and P-MapNet [5] obtaining the baseline and the S+H module. To ensure fairness in the experimental results, all methods underwent the same pre-training process: applying a 50% probability random mask to the ground truth and iterating through 20 epochs in the pre-training phase, followed by 10 epochs of fine-tuning. The experimental results in Table I show that our method not only achieves state-of-the-art performance but also shows superior performance in handling

TABLE IV: Different sampling methods and steps to generate semantic segmentation in the range of  $120 \times 60m$ .

Type	Step	Div.	Ped.	Bound.	mIoU (%)
DDIM	3	47.30	33.10	47.40	<b>42.60</b>
DDIM	1	47.30	33.10	47.30	42.57
DDPM	1000	47.20	33.20	47.30	42.57

TABLE V: Analyses of the effects of pretraining in different perception ranges.

Range (m)	Pretrain	Div.	Ped.	Bound.	mIoU (%)
60×30	-	44.30	23.30	43.80	37.13
	✗	45.30	24.70	45.10	38.40
	✓	<b>45.90</b>	<b>25.80</b>	<b>45.40</b>	<b>39.03</b>
120×60	-	45.50	30.90	46.20	40.87
	✗	46.20	31.20	46.80	41.43
	✓	<b>47.30</b>	<b>33.20</b>	<b>47.30</b>	<b>42.60</b>
240×60	-	49.00	40.90	46.60	45.50
	✗	49.90	41.20	48.30	46.47
	✓	<b>51.60</b>	<b>43.90</b>	<b>49.60</b>	<b>48.37</b>

long-distance segmentation issues, with a specific improvement of 2.87% in accuracy. This enhancement highlights the superiority of our method in addressing challenging long-distance segmentation tasks. Fig. 4 demonstrates that our method enhances the recovery of semantic maps across the BEV HD mapping tasks. Ours has a higher improvement for pedestrian crossing, which helps to enhance the reliability of perception towards safe autonomous driving.

**BEV Semantic Mapping.** Given that the road information covered by the HD mapping task is not comprehensive enough, we attempt to assess BEV semantic mapping to achieve a more thorough analytical outcome. To ensure the fairness of the experiments, we replace the original LSS [11] generation method in DDP [6] with the IPM [12] approach used in our method and integrate the baseline with the DDP framework. We train the combined model using the same pre-training and fine-tuning procedures as ours. The results demonstrate that ours significantly outperforms the generation approach of DDP, achieving an improvement of 1.92% over the results generated by P-MapNet.

### C. Ablation Study

**Ablation of TS-CGNet Modules.** As shown in Table III, we conduct ablation studies to assess the effectiveness of the proposed module for the BEV HD mapping task within the perception range of  $120 \times 60m$ . The results demonstrate that system performance improves incrementally with the addition of each module, reaching a saturation point due to limitations imposed by the fixed parameters in the local mapping system, which restrict the richness of feature extraction.

**Ablation of Sampling Methods.** To evaluate the impact of different sampling methods on map generation, we perform ablation experiments for the BEV HD mapping task within a perception range of  $120 \times 60m$  in Table IV. We employ the sampling method from [6] and compare the efficiency of image generation between DDIM and DDPM. The results indicate that the model achieves the highest accuracy with only 3 sampling steps. Even with a single step of generation,

TABLE VI: Robustness evaluation for semantic mapping under the weather conditions using the metric of mIoU (%).

Type	Level	P-MapNet [5]	Ours	Progress (%)
Brightness	Easy	44.47	47.40	+2.93
	Mid	42.47	45.57	+3.10
	Hard	42.30	45.33	+3.03
Dark	Easy	42.63	45.33	+2.70
	Mid	42.57	45.07	+2.50
	Hard	42.43	45.13	+2.70
Fog	Easy	43.80	46.87	+3.07
	Mid	43.47	46.60	+3.13
	Hard	43.27	46.33	+3.06
Snow	Easy	44.97	47.87	+2.90
	Mid	43.93	46.97	+3.04
	Hard	44.03	47.00	+2.97

TABLE VII: Robustness evaluation for semantic mapping under the sensor interferences using the metric of mIoU (%).

Type	Level	P-MapNet [5]	Ours	Progress (%)
FrameLost	Easy	44.80	47.90	+3.10
	Mid	43.73	47.00	+3.27
	Hard	43.20	46.30	+3.10
MotionBlur	Easy	45.53	48.37	+2.84
	Mid	45.43	48.30	+2.87
	Hard	45.37	48.27	+2.90
CameraCrash	Easy	44.47	47.30	+2.83
	Mid	44.47	47.27	+2.80
	Hard	44.57	47.53	+2.96
ColorQuant	Easy	45.57	48.27	+2.70
	Mid	45.53	48.30	+2.77
	Hard	44.60	47.47	+2.87

the model can attain a sufficiently effective accuracy level, consistent with the framework [6] expectations. Since the DDPM method in [6] averages the predicted masks across random steps to generate the final output after the diffusion process, the resulting outputs vary in quality. This variation leads to an acceptable reduction in precision.

**Ablation of Pretraining.** As shown in Table V, we conduct experiments with direct fine-tuning across 3 perception ranges. Without pretraining, the accuracy of ours still improves by 1.27%, 0.56%, and 0.97% compared with the SOTA method. This result further confirms the effectiveness of ours. Furthermore, when combined with pretraining, our approach demonstrates even more significant advantages, with the accuracy gain expanding to 1.87%, 1.73%, and 2.87%. This significant leap in performance demonstrates that our innovative architecture can effectively harness pre-trained knowledge. By leveraging the core functionality of the CGDM module, it restores and reconstructs semantic segmentation maps, thereby markedly enhancing the quality of map generation.

### D. Robustness Analysis

To address the critical challenges in autonomous driving perception, we systematically evaluate our performance under 8 distinct weather and sensor conditions that directly reflect real-world operational scenarios. These damage situations fall into two categories, namely environmental disturbances (*i.e.*, *Brightness*, *Dark*, *Fog*, and *Snow*), and hard-

ware failures (i.e., *CameraCrash*, *MotionBlur*, *FrameLost*, *ColorQuant*).

In the experiments conducted within a  $240 \times 60m$  perception range in Table VI, VII, our method achieves an average accuracy improvement of 2.92% across all fault types. Notably, under *FrameLoss* conditions, leveraging historical prior information and road centerline guidance, our method realizes precision gains of 3.10%, 3.27%, and 3.10% at *easy*, *medium*, and *hard* difficulty levels, respectively. As shown in Fig. 4, we display our capability in map generation during nighttime. It can be observed that our predictions for corners and further distances are more complete.

Furthermore, the method exhibits the capability to mitigate other types of faults to varying extents. This capability fundamentally enhances the operational reliability of autonomous driving systems when encountering unpredictable environmental conditions and establishes a new solution for the safety of real-world deployment.

## V. CONCLUSION

In this paper, we present a TS-CGNet framework leveraging temporal-spatial fusion and centerline-guided diffusion for performing BEV perception. The core insight is to utilize learned generative priors as well as historical information as the prompt and centerline as the condition to provide diverse and accurate layout estimates, which provide good map conditions for more informed decision-making and path planning. Our experiments show that we produce more realistic scene layouts with improved accuracy. In the future, we will aim to complete long-term sequential tasks and evaluate the potential of our solution on global maps.

## REFERENCES

- [1] Z. Liu *et al.*, “BEVFusion: Multi-task multi-sensor fusion with unified bird’s-eye view representation,” in *Proc. ICRA*, 2023, pp. 2774–2781.
- [2] Z. Li *et al.*, “BEVFormer: Learning bird’s-eye-view representation from LiDAR-camera via spatiotemporal transformers,” *IEEE Transactions on Pattern Analysis and Machine Intelligence*, 2024.
- [3] A. W. Harley, Z. Fang, J. Li, R. Ambrus, and K. Fragkiadaki, “Simple-BEV: What really matters for multi-sensor bev perception?” in *Proc. ICRA*, 2023, pp. 2759–2765.
- [4] Z. Yang *et al.*, “MapVision: CVPR 2024 autonomous grand challenge mapless driving tech report,” *arXiv preprint arXiv:2406.10125*, 2024.
- [5] Z. Jiang *et al.*, “P-MapNet: Far-Seeing map generator enhanced by both SDMap and HDMap priors,” *IEEE Robotics and Automation Letters*, vol. 9, no. 10, pp. 8539–8546, 2024.
- [6] Y. Ji *et al.*, “DDP: Diffusion model for dense visual prediction,” in *Proc. ICCV*, 2023, pp. 21 684–21 695.
- [7] Q. Li, Y. Wang, Y. Wang, and H. Zhao, “HDMapNet: An online HD map construction and evaluation framework,” in *Proc. ICRA*, 2022, pp. 4628–4634.
- [8] H. Caesar *et al.*, “nuScenes: A multimodal dataset for autonomous driving,” in *Proc. CVPR*, 2020, pp. 11 618–11 628.
- [9] S. Xie *et al.*, “Benchmarking and improving bird’s eye view perception robustness in autonomous driving,” *IEEE Transactions on Pattern Analysis and Machine Intelligence*, 2025.
- [10] M. Tan and Q. Le, “EfficientNet: Rethinking model scaling for convolutional neural networks,” in *Proc. ICML*, 2019, pp. 6105–6114.
- [11] J. Phillion and S. Fidler, “Lift, splat, shoot: Encoding images from arbitrary camera rigs by implicitly unprojecting to 3D,” in *Proc. ECCV*, vol. 12359, 2020, pp. 194–210.
- [12] L. Deng, M. Yang, H. Li, T. Li, B. Hu, and C. Wang, “Restricted deformable convolution-based road scene semantic segmentation using surround view cameras,” *IEEE Transactions on Intelligent Transportation Systems*, vol. 21, no. 10, pp. 4350–4362, 2020.
- [13] T. Sämann, K. Amende, S. Milz, C. Witt, M. Simon, and J. Petzold, “Efficient semantic segmentation for visual bird’s-eye view interpretation,” in *Proc. IAS*, 2019, pp. 679–688.
- [14] S. Li *et al.*, “Bi-Mapper: Holistic BEV semantic mapping for autonomous driving,” *IEEE Robotics and Automation Letters*, vol. 8, no. 11, pp. 7034–7041, 2023.
- [15] D. Duckworth *et al.*, “SMERF: Streamable memory efficient radiance fields for real-time large-scene exploration,” *ACM Transactions on Graphics*, vol. 43, no. 4, pp. 1–13, 2024.
- [16] J. Liu, X. Huang, Y. Liu, and H. Li, “MixMIM: Mixed and masked image modeling for efficient visual representation learning,” *arXiv preprint arXiv:2205.13137*, 2022.
- [17] K. Wu, S. Nian, C. Shen, C. Yang, and Z. Li, “LGmap: Local-to-global mapping network for online long-range vectorized HD map construction,” *arXiv preprint arXiv:2406.13988*, 2024.
- [18] M. Haklay and P. Weber, “OpenStreetMap: User-generated street maps,” *IEEE Pervasive Computing*, vol. 7, no. 4, pp. 12–18, 2008.
- [19] H. Wu *et al.*, “BLOS-BEV: Navigation map enhanced lane segmentation network, beyond line of sight,” in *Proc. IV*, 2024, pp. 3212–3219.
- [20] X. Xiong, Y. Liu, T. Yuan, Y. Wang, Y. Wang, and H. Zhao, “Neural map prior for autonomous driving,” in *Proc. CVPR*, 2023, pp. 17 535–17 544.
- [21] T. Yuan, Y. Liu, Y. Wang, Y. Wang, and H. Zhao, “StreamMapNet: Streaming mapping network for vectorized online HD map construction,” in *Proc. WACV*, 2024, pp. 7341–7350.
- [22] A. Shi, Y. Cai, X. Chen, J. Pu, Z. Fu, and H. Lu, “GlobalMapNet: An online framework for vectorized global HD map construction,” *arXiv preprint arXiv:2409.10063*, 2024.
- [23] S. Li *et al.*, “DTCLMapper: Dual temporal consistent learning for vectorized HD map construction,” *IEEE Transactions on Intelligent Transportation Systems*, vol. 25, no. 12, pp. 21 672–21 686, 2024.
- [24] D. P. Kingma and M. Welling, “Auto-encoding variational bayes,” in *Proc. ICLR*, 2014.
- [25] A. Van den Oord and J. Kautz, “NVAE: A deep hierarchical variational autoencoder,” in *Proc. NeurIPS*, vol. 33, 2020, pp. 19 667–19 679.
- [26] N. Parmar *et al.*, “Image transformer,” in *Proc. ICML*, vol. 80, 2018, pp. 4052–4061.
- [27] K. He, X. Chen, S. Xie, Y. Li, P. Dollár, and R. Girshick, “Masked autoencoders are scalable vision learners,” in *Proc. CVPR*, 2022, pp. 15 979–15 988.
- [28] X. Zhu, V. Zyrianov, Z. Liu, and S. Wang, “MapPrior: Bird’s-eye view map layout estimation with generative models,” in *Proc. ICCV*, 2023, pp. 8194–8205.
- [29] P. Dhariwal and A. Nichol, “Diffusion models beat GANs on image synthesis,” in *Proc. NeurIPS*, vol. 34, 2021, pp. 8780–8794.
- [30] J. Ho, A. Jain, and P. Abbeel, “Denoising diffusion probabilistic models,” in *Proc. NeurIPS*, vol. 33, 2020, pp. 6840–6851.
- [31] R. Rombach, A. Blattmann, D. Lorenz, P. Esser, and B. Ommer, “High-resolution image synthesis with latent diffusion models,” in *Proc. CVPR*, 2022, pp. 10 674–10 685.
- [32] L. Zhang, A. Rao, and M. Agrawala, “Adding conditional control to text-to-image diffusion models,” in *Proc. ICCV*, 2023, pp. 3813–3824.
- [33] P. Jia, T. Wen, Z. Luo, M. Yang, K. Jiang, Z. Liu, X. Tang, Z. Lei, L. Cui, B. Zhang *et al.*, “Diffmap: Enhancing map segmentation with map prior using diffusion model,” *IEEE Robotics and Automation Letters*, 2024.
- [34] J. Long, E. Shelhamer, and T. Darrell, “Fully convolutional networks for semantic segmentation,” in *Proc. CVPR*, 2015, pp. 3431–3440.
- [35] O. Ronneberger, P. Fischer, and T. Brox, “U-Net: Convolutional networks for biomedical image segmentation,” in *Proc. MICCAI*, vol. 9351, 2015, pp. 234–241.
- [36] M. Jaderberg, K. Simonyan, A. Zisserman, and K. Kavukcuoglu, “Spatial transformer networks,” in *Proc. NeurIPS*, vol. 28, 2015, pp. 2017–2025.
- [37] T.-Y. Lin, P. Goyal, R. Girshick, K. He, and P. Dollár, “Focal loss for dense object detection,” in *Proc. ICCV*, 2017, pp. 2999–3007.
- [38] T. Roddick, A. Kendall, and R. Cipolla, “Orthographic feature transform for monocular 3d object detection,” *arXiv preprint arXiv:1811.08188*, 2018.